DISTRIBUTION OF GOLD IN TIN-RICH SAMPLES
FROM THE CORVO OREBODY, PORTUGAL

LOUIS J. CABRI[1]

CANMET – MMSL, 555 Booth Street, Ottawa, Ontario K1A 0G1

ORLANDO C. GASPAR[1]

Laboratório do Instituto Geológico e Mineiro, Apartado 1089, P-4465 S. Mamede de Infesta, Portugal

ROLANDO LASTRA[1]

CANMET – MMSL, 555 Booth Street, Ottawa, Ontario K1A 0G1

GREG McMAHON[1]

CANMET – MTL, 568 Booth Street, Ottawa, Ontario K1A 0G1

ABSTRACT

The mineralogical distribution of gold in samples from the Corvo orebody, in the Iberian Pyrite Belt of Portugal, was determined in a detailed study of a few hand samples of RT ("rubané tin") ore. In one sample, 42% of the gold occurs invisibly in pyrite I, pyrite II, and arsenopyrite, with the balance assumed to be carried by cassiterite, which makes up 56.5 wt.% of the sample. Extrapolation of these results to a sample of high-grade tin concentrate (68.99 wt.% Sn) suggests that cassiterite in the concentrate contains about 149 ppb Au, representing 88% of the total gold in the concentrate. These results have implications on the metallogeny of the Neves–Corvo volcanogenic massive sulfide deposit as well as on the metallurgical treatment of the ores.

Keywords: Corvo, Neves–Corvo, volcanogenic massive sulfide, Iberian Pyrite Belt, invisible gold, ore mineralogy, pyrite, arsenopyrite, cassiterite, secondary-ion mass spectrometry (SIMS), image analyses, metallogeny, metallurgy, Portugal.

SOMMAIRE

Nous avons déterminé la distribution de l'or dans des échantillons de minerai provenant du gisement de Corvo, dans la ceinture ibérique de pyrite, au Portugal, dans une étude détaillée de quelques échantillons de minerai stannifère RT. Dans un échantillon, 42% de l'or est présent sous forme invisible dans la pyrite de première génération, la pyrite de deuxième génération, et l'arsenopyrite, le reste étant incorporé dans la cassitérite, qui constitue 56.5% (base pondérale) de l'échantillon. D'après une extrapolation de ces résultats au cas d'un échantillon du concentré enrichi d'étain (68.99% Sn, par poids), la cassitérite du concentré contiendrait environ 149 ppb Au, ce qui représente 88% de l'or présent dans le concentré. Ces résultats ont des implications importantes pour la métallogenie du gisement de sulfures massifs volcanogéniques de Neves–Corvo, de même que pour le traitement métallurgique du minerai.

(Traduit par la Rédaction)

Mots-clés: Corvo, Neves–Corvo, sulfures massifs volcanogéniques, ceinture ibérique de pyrite, or invisible, minéraux des minerais, pyrite, arsenopyrite, cassitérite, spectrométrie de masse des ions secondaires (SIMS), analyse d'images, métallogénie, métallurgie, Portugal.

[1] *E-mail addresses*: lcabri@nrcan.gc.ca, orlando.gaspar@igm.pt, rlastra@nrcan.gc.ca, gmcmahon@nrcan.gc.ca

INTRODUCTION

The Neves–Corvo volcanogenic massive sulfide (VMS) deposit, discovered in 1977 in southern Portugal, consists of a cluster of five polymetallic orebodies (Neves, Neves-Norte, Lombador, Corvo and Graça) linked by thin bridges of massive cupriferous ores. The deposit is one of some 80 sulfide deposits found to date in the Iberian Pyrite Belt (IPB), shown in Figure 1. The IPB is a major geotectonic unit of the Iberian segment of the Hercynian fold belt, containing an estimated total of 1,300 M tonnes of sulfide reserves (ore mined + reserves) grading 0.92% Cu, 0.77% Pb, 2.33% Zn, 0.58 g/t Au, and 29 g/t Ag (Leistel *et al.* 1994). Resources of precious metals of the IPB are significant, with an estimated 920 t Au and 49,400 t Ag (Leistel *et al.* 1994, 1998b). The Neves–Corvo deposit is one of the largest deposits of the IPB, containing approximately 300 Mt of massive sulfides that are locally very rich in copper and tin. It is currently the largest producer of Cu and Sn in Europe, with 1.092 Mt Cu and 26,200 t Sn produced from 1988 to 1997 (Real & Carvalho 1997).

In this paper, we present and discuss the results of limited bulk assays, microscopy, image analysis and ion-microprobe analyses (SIMS) of minerals in hand samples of RT ("rubané" tin) ore from the Corvo orebody (Gaspar 1998), as well as from a sample of high-grade tin concentrate.

BACKGROUND INFORMATION

Most of the Corvo orebody is overlain by the so-called "rubané" ores (Figs. 2, 3) that formed from systems of veins, consisting either of banded chalcopyrite or cassiterite, both having developed within a deformed shale horizon that was extensively altered to a fine-grained quartz – chlorite assemblage. The cassiterite-bearing veins encompass a number of types, both in
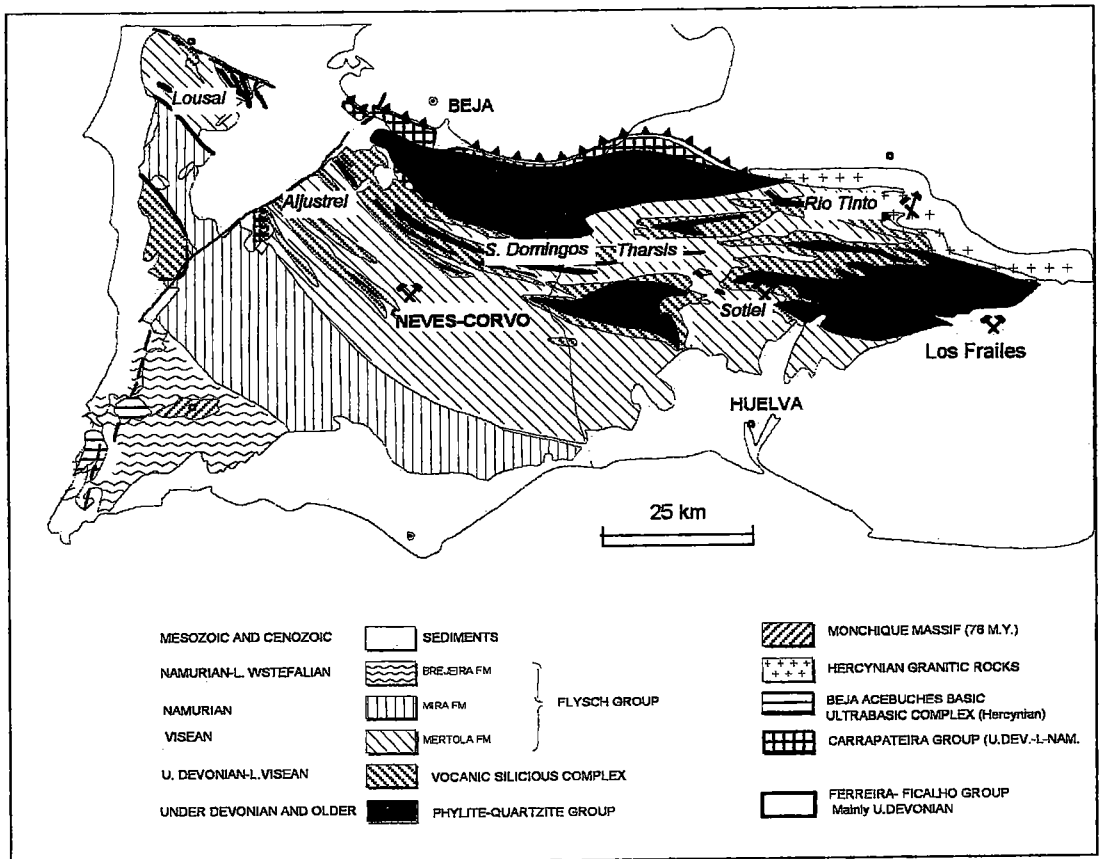

FIG. 1. General geology of the Iberian Pyrite Belt and location of the Neves–Corvo massive sulfide deposit, as well as the Aljustrel deposit (slightly modified from Carvalho *et al.* 1976).
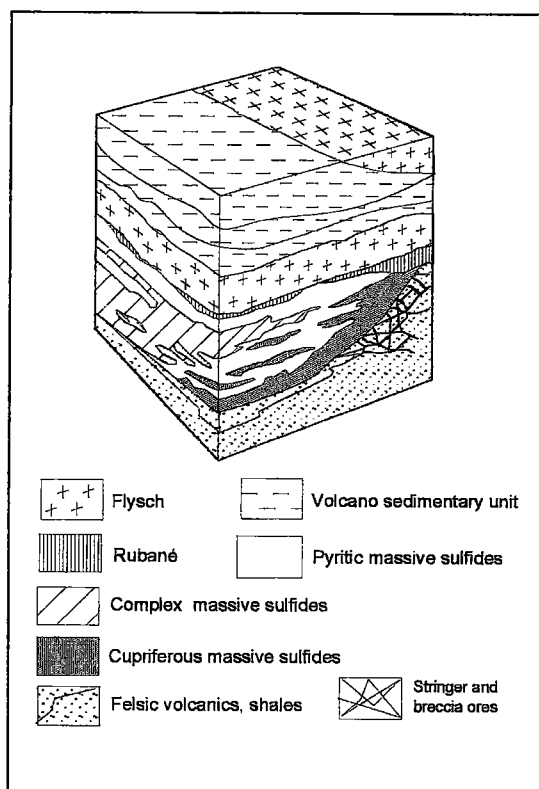
Flysch

Rubané

Complex massive sulfides

Cupriferous massive sulfides

Felsic volcanics, shales

Volcano sedimentary unit

Pyritic massive sulfides

Stringer and breccia ores

FIG. 2. Simplified block diagram of the Neves–Corvo orebody showing the different types of ore occurring in the deposit (SOMINCOR, unpubl. report, 1989). The *rubané ore* consists of thin-banded alternations of shales with layers and cross-cutting veinlets of cassiterite and sulfides (mostly chalcopyrite and pyrite). The *rubané* has been tectonically placed mainly at the top of the massive sulfides of the Corvo orebody (see Fig. 3). The *pyritic sulfide ore* consists mainly of pyrite and has Cu + Zn + Pb contents lower than 2%. The *complex massive ore* is a polymetallic base-metal ore rich in sphalerite and with Cu contents lower than 2%. The *cupriferous massive ore* consists mainly of chalcopyrite (>2% Cu) and pyrite along with accessory sphalerite, cassiterite, sulfides of Sn and tetrahedrite–tennantite. The *stringer* and *breccia ores* consist of stockwork-type mineralization that locally can be rich in chalcopyrite (>2% Cu) or cassiterite (>1% Sn), and which cut across the black shales or the felsic volcanic rocks of the footwall.

increasing degree of complexity of their constituent minerals and textural relationships. The veins show evidence of repeated opening and limited movement that resulted in extensive fracturing of their constituent minerals. Local shearing and the introduction of later stages of mineralization superimposed upon the earlier cassiterite-rich assemblages were observed. Cassiterite

is an early phase, generally intergrown with quartz and siderite or dolomite. The cassiterite crystals are euhedral to subhedral and are commonly markedly elongate or prismatic. Individual crystals range between 15 μm and 2 mm in size, and are commonly fractured. Their color in transmitted light varies between light reddish brown and pale yellow, and both compositional zoning and signs of strong deformation are widespread (Gaspar 1991). The iron content can vary either in the same or between different crystals. Zoning in cassiterite was confirmed by Serranti (1998), who reported on 11 cassiterite grains with Fe contents ranging from 0.25 to 2.19 wt% FeO, as determined by electron-probe microanalyses. In addition, Serranti *et al.* (1997) reported results of trace-element analyses by micro-PIXE on several ore minerals from the Corvo orebody and found that cassiterite contains maximum values (in ppm) of 919 Cu, 136 Zn, 15 Ga, 41 As, 394 In, 243 Sb, 261 Te, 98 Ta and 11,119 W. Two cassiterite crystals that show no growth zoning were reported by Neiva (1996) to contain 0.18 wt% FeO (in a pale yellow crystal) and 1.93 wt% FeO (in a brown crystal). Significant amounts of pyrite were introduced toward the waning stages of cassiterite precipitation. A later period of mineralization, connected to extensive fracturing, resulted in complex chalcopyrite – stannite – tetrahedrite – pyrite assemblages. Minor amounts of arsenopyrite, chalcopyrite, sphalerite, galena and löllingite have been observed sporadically within the ores. Signs of a reaction between cassiterite crystals and later fluids carrying sulfides also are observed, in some cases producing a stannite halo. Cassiterite is usually replaced by stannite. The so-called cupriferous RC "rubané" ore is characterized by alternating bands of slate and laminated chalcopyrite that shows recrystallization and strong deformation, with the development of twins in some crystals.

Hennigh (1996), Hennigh & Hutchinson (1997) and Relvas *et al.* (1997) assumed that the "rubané" tin (RT) and "rubané" copper ores (RC) were displaced from their original positions mainly because of gravity flow by syntectonic mechanisms during the late stages of ore deposition. However, detailed macro- and microtextural studies of both ores and slates by one of us (O.C.G.) suggest that the "rubané" ores have also suffered both strong deformation and significant transport, mainly due to later Hercynian tectonic activity. The original smectite-rich sediments, as a result of both diagenesis and low-grade metamorphism, have been altered to a shale horizon that varies between dark olive green and dark gray in color, consisting mainly of quartz and a chlorite, close in composition to chamosite. Small amounts of fine-grained rutile are disseminated throughout the shale, occurring as aggregates of tiny micrometer-sized grains elongate parallel to the bedding of the shale. Dolomite may be present both as isolated grains and narrow layers developed within the shale. Hydrothermal alteration of the shale can also be observed in the immediate vicinity of mineralized fractures, which
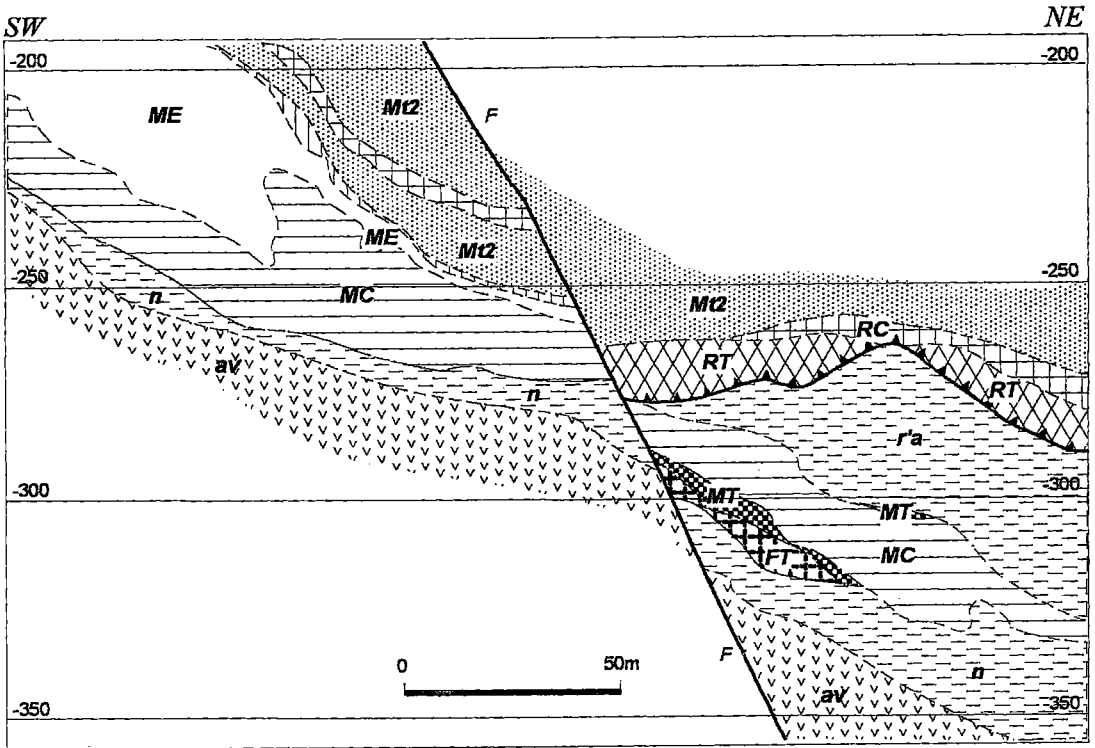
FIG. 3. Corvo orebody cross-section (SOMINCOR, unpubl. report, 1996). Lithologic sequence: Mt2: greywakes and shales of the Mértola Formation, RC: rubané copper ore, RT: rubané tin ore, ME: massive pyritic ores with lower base-metal contents, MC: massive cupriferous ores, r'a: black pyritic shale, MT: massive tin ore, FT: stringer tin ore, n: black shale of the Neves Formation, v: felsic volcanic rocks. All the samples studied were collected from the Corvo rubané tin ore (RT).

commonly occur close to the mineralized sulfide veins.

There is some information published about the occurrence or distribution of gold in the Neves–Norte and Lombador orebodies (Ferreira *et al.* 1997, Pinto *et al.* 1994, 1995, 1997), and none on the Corvo orebody. To date, the exploitation of massive sulfide ores at Neves–Corvo has been restricted to the rich copper and tin ores (see Table 1 for the definition of economic ore-types based on their cut-off grades). Gold contents in these massive cupriferous ores (MC ores) are mostly very low (< 0.5 g/t). However, significant amounts of visible gold were found for the first time in the stringers of the zinciferous massive MZ ores (Table 1) of the Lombador orebody and in the lower part of the cupriferous massive MC ores that are located at the top of stringer ores of Neves–Norte and Corvo orebodies. Brief descriptions of these gold occurrences have recently been given by Ferreira *et al.* (1997) and Pinto *et al.* (1997). One of us (Gaspar 1996) assumes that the mineralogical associations of gold described by these investigators (Tables 2, 3) represent a paragenesis later than the massive

sulfides, related to reactivated NE-trending faults. The gold content in the zinciferous MZ massive sulfides has not, to date, been systematically estimated, but it is assumed by the mine personnel to be mostly lower than 1 g/t.

The stringer ores of the Lombador orebody were intersected by drilling in 1991. Fire assays of drill-core

TABLE 1. ORE TYPES ESTABLISHED AT THE NEVES–CORVO MINE ON THE BASIS OF CUT-OFF GRADES*

ORE TYPES		CUT-OFF GRADES
RT	"Rubané" ores with tin	$Sn \geq 1\%$
FT	*Fissural* (stringer) ores with tin	$Sn \geq 1\%$
MS	cupriferous massive sulfide ores with tin	$Cu > 2\%, Sn \geq 1\%$
MC	cupriferous massive sulfide ores	$Cu > 2\%, Sn < 1\%$
RC	cupriferous "rubané" ores	$Cu > 2\%, Sn < 1\%$
FC	cupriferous *fissural* (stringer) ores	$Cu > 2\%, Sn < 1\%$
MZ	massive sulfides ores rich in zinc	$Zn \geq 3.3\%$
ME	massive pyritic ores	$Zn < 1\%, Cu < 2\%, Sn < 1\%$

* Data from SOMINCOR and Oliveira *et al.* (1997).

TABLE 2. SUMMARY OF MINERAL ASSOCIATIONS
RICH IN In, Hg, Ag, Au, Te, Sn AND Sb, FOUND BY DRILLING
IN STRINGER ORES AT THE LOMBADOR OREBODY§

Elements	Main carriers of elements in the stringer ores
Co	Glaucodot* [(Co,Fe)AsS] highly zoned crystals containing 8 to 27% Co, and 25% As Cobaltite [CoAsS] contains 30.9 to 32.6% Co Alloclasite* [(Co,Fe)AsS] intergrown with arsenopyrite (0.4% Co) contains about 19% Co
Bi	Native bismuth as skeletal crystals containing virtually 100% Bi Bismuthinite [(Bi,Pb,Cu)$_{1.98}$(S,Sb)$_{3.02}$] contains 1.2–3.5% Sb and 69–79% Bi "Rezbanyite"* [(Cu,Ag,Co)$_{4.3}$Pb$_{2.9}$(Bi,Hg)$_{9.3}$S$_{19.0}$] contains 55–59% Bi, 0.4% Hg, 1.3% Co, 0.7–1.3% Sb, and <100 ppm In Galenobismuthinite [PbBi$_2$S$_4$] interstitial to pyrite and cobaltite, contains 0–0.5% Ag, 1.9–3% Sb, 0–0.25% Te and 43–49% Bi
Bi, Te	Tetradymite [Bi$_2$Te$_2$S] contains 35% Te and 59% Bi Joséite-B [Bi$_4$Te$_2$S] contains 23% Te and 73% Bi
Sb, Ag	Tetrahedrite [(Cu$_{9.8}$Ag$_{0.2}$)$_{\Sigma10}$(Fe$_{0.8}$Zn$_{1.1}$)$_{\Sigma1.9}$(Sb$_{3.8}$As$_{0.1}$)$_{\Sigma4.0}$S$_{12.9}$] contains 0.76–1.15% Bi, 0.42–1.33% Ag
In	Sphalerite [(Zn,Fe)S] contains 0.78 to 1.04% In, and 0.19 to 0.29% Cd Cassiterite [SnO$_2$] contains about 0.18% In
Au	Native gold: associated with arsenopyrite (87% Au, 11.8% Ag, 0.3–0.7% Hg), with cobaltite and "rezbanyite" (80% Au, 5–18% Ag, 0.6–1.7% Hg), and with tetrahedrite and galena (75% Au, 20–22% Ag and 3–5% Ag)

§ Sources: SOMINCOR SA, Mineral Science Ltd. (UK), Pinto *et al.* (1994, 1995, 1997) and internal reports. * Note that alloclasite and glaucodot were identified by their optical properties. "Rezbanyite" is considered a mixture.

TABLE 3. MINERAL CHEMISTRY OF AN UNUSUAL PARAGENESIS
ASSOCIATED WITH BORNITE IN NEVES NORTE (MC ORES),
CORVO (MC ORES), AND GRAÇA (MC AND CUPRIFEROUS MH ORES)*

Mineral	Chemical composition in the reaction zone of MC
Bornite	(Cu,Ag)$_{4.93}$Fe$_{0.97}$S$_{4.10}$
Mawsonite	Cu$_{5.95}$Fe$_{2.01}$Sn$_{1.00}$S$_{8.05}$

In-Bi-Hg-enriched
    Tennantite
	(Cu,Ag,Fe,Zn,Hg,In)$_{\Sigma11.76}$(As,Sb,Bi)$_{\Sigma4.1}$S$_{13.24}$
	    containing 0.9 to 2.7% In, ≤8.0% Bi and ≤1.0% Hg

Vinciennite	Cu$_{10.53}$Fe$_{3.81}$Sn$_{0.99}$(As,Sb,Ag)$_{0.99}$S$_{15.72}$
Wittichenite	(Cu,Fe,Ag)$_{\Sigma3.01}$Bi$_{1.01}$S$_{2.98}$ contains up to 1.8% Ag
Miharaite	(Cu,Ag)$_{4.00}$Fe$_{0.96}$Pb$_{0.96}$Bi$_{1.02}$S$_{6.06}$ contains up to 1.2% Ag
Carrollite	Cu$_{0.97}$(Co,Ni,Fe)$_{\Sigma1.96}$S$_{4.07}$
Cobaltian pyrite	(Fe,Co,Cu,Ni)$_{\Sigma1.09}$S$_{1.91}$, with ≤7.5% Co
Galena – Clausthalite	Pb$_{0.95}$(S,Se)$_{\Sigma1.00}$
Galena	contains about 14% Bi and an average of about 14% of the clausthalite (PbSe) component
Naumannite	Ag$_{1.95}$Se$_{0.94}$
Stromeyerite (?)	AgCuS
Colusite	(Cu,Ag)$_{\Sigma26.83}$V$_{1.56}$(As,Sn,Sb,Fe)$_{\Sigma6.57}$S$_{31.00}$
Gold	Au grains (<10 µm) with variable quantities of Ag

* Sources: SOMINCOR SA, Mineral Science Ltd. (UK), LEM-GESD, ENSG (France), Laboratório do IGM (Portugal), Pinto *et al.* (1994, 1995, 1997).

intersections show contents of 15 g/t Au over 3 meters with a value of 22.6 g/t for the central one-meter of core, and 94.5 g/t for the richest part. In 1994, a one-meter drill core intersection of the Neves-Norte cupriferous massive ores (MC), located at the top of stringer zones, had assays up to 10 g/t Au, and as much as 33 g/t over 0.2 m of core. The gold occurs along with unusual mineral assemblages found in these two orebodies (Tables 2, 3). Recently, similar gold mineralization has also been found in the *bridge* of cupriferous ores that links the Corvo and Graça orebodies.

Ore-microscope and electron-probe studies on these unusual mineralogical associations (Tables 2, 3) have been jointly carried out since 1994 by the mineralogical laboratory of SOMINCOR (Neves–Corvo), Laboratório do IGM (Portugal), Mineral Sciences Ltd (U.K.) and Laboratoire de L'Environnement et Minéralurgie (LEM–GESD ENSG, Nancy, France), in the context of the research project "New Integrated Flowsheets for Separation and Recovery of Minor Elements from Sulfides – Brite-Euram II Program" funded by the European Union. The consortium has characterized a large bornite-rich zone in the Neves–Norte orebody, unusually enriched in Cu, Sn, Bi, Co, In, Hg, Se, Ag and Au, which had never previously been found in any of the ore deposits of the IPB (Table 3). Bornite occurs, along with tennantite, mawsonite and stannoidite, in addition to abundant chalcopyrite. Other ore minerals include

miharaite, carrollite, vinciennite, galena, colusite, stromeyerite, arsenopyrite, sphalerite, tetrahedrite, and naumannite (occurring as exsolution-induced blebs in galena). Native gold occurs in naumannite, which is associated with wittichenite, but the grains of gold are too small for analysis by electron microprobe. However, bulk analyses of the ores by fire assay show contents between 0.2 and 10 ppm Au. Subhedral to euhedral grains of quartz form the main portion of the main gangue minerals. Carbonate, dolomite and low-iron siderite veins cut across the stringer mineralization.

There is a clear similarity between the bornite zone found at the Neves–Norte orebody and the bornite-rich ores of the Kidd Creek deposit described by Hannington *et al.* (1997). Also similar is the North Lyell section of Mt. Lyell massive sulfide ores (Markham 1968), where tennantite, galena, copper sulfides, mawsonite, stromeyerite and wittichenite (?) are associated with chalcopyrite–bornite ores. At Kidd Creek, as at Mt. Lyell, Bi–Se sulfides are also common in the stringer zones.

Marcoux & Leistel (1996) and Leistel *et al.* (1998a, b) reviewed the mineralogy and geochemistry of many Spanish VMS of the IPB and made some observations on three Portuguese ore deposits. They reported that these deposits generally contain from 1 to 1.5 g/t Au (exceptionally up to 50 g/t), but with weaker Au grades in the massive sulfides of the Portuguese deposits. Grades of gold seldom exceed 1 g/t in the Zn – Pb ± Ag massive sulfides of the Aljustrel deposit (Fig. 1) and are mostly ≤0.5 g/t in the cupriferous massive MC sulfide

ores in Corvo, Graça and Neves–Norte orebodies (data provided, respectively, by Pirites Alentejanas SA and SOMINCOR SA).

Detailed mineralogical and geochemical studies of IPB deposits in Spain led Leistel *et al.* (1998b) to define two types of gold association: (a) an early higher-temperature (>300°C) association of Au (with Co ± Bi) enriched in stockworks and zones of interaction at the base of the sulfide mounds, and (b) a later, lower-temperature (<280°C) generation of Au enriched in polymetallic sulfides (Zn + Ag ± As ± Tl ± Hg) in a distal position or beneath massive sulfides. The gold is reported to usually occur in the first association as small (<10 μm) grains of electrum associated with Bi minerals, as inclusions within cobaltite or alloclasite, or attached to cobalt minerals in chalcopyrite. The Au in the second association occurs as electrum and gold-bearing needle-shaped arsenopyrite and pyrite within a polymetallic association (predominantly Pb–Zn). Leistel *et al.* (1998b) also briefly reported results of laser-ablation microprobe – inductively coupled plasma – mass spectrometry (LAM–ICP–MS) of arsenopyrite with gold contents ranging between 15 and 3,150 ppm (average 280 ppm) and between 200 and 500 ppb in pyrite (done by Bob Nesbitt, Southampton; E. Marcoux, pers. commun., April 1998).

SAMPLES

Eight of the samples studied are representative of the tin-rich ores, seven of which were collected by the second author between 1990 and 1992 from different locations in the Corvo orebody. One sample is a grab-sample of high-grade tin concentrate collected at the tin processing plant in September 1997 from a shipping bin. Because the tin plant concentrates cassiterite from two different types of ore (MS and RT), the sample collected probably represents a mixture of two different types of cassiterite.

Eight samples represent different forms of occurrence and mineralogical associations of the so-called *rubané* ores that overlap the top of the Corvo massive sulfides. Samples IGM#1, IGM#5, IGM#6 and IGM#7 were collected in the *rubané* mineralized horizon, which mainly consists of a strongly chloritized shale with banded intercalations of chalcopyrite and pyrite. However, in some places the shale is rich in *boudins* or clusters of centimeter-sized crystals of cassiterite that are invariably recrystallized and strongly brecciated. No direct quantitative correlation between cassiterite and sulfides occurrences has, so far, been established.

In a broad sense, the samples IGM#1, IGM#5, IGM#6 and IGM#7 represent different types of *rubané* ores: sample IGM#1 corresponds to a more abundant type showing pyrite along with chalcopyrite cutting across the chloritic shale. A banded texture is only visible whenever the chalcopyrite content strongly increases, allowing a more plastic deformation. Sample

IGM#5, which corresponds to a strongly deformed shale, contains clasts of siderite and cassiterite in a matrix of later chalcopyrite. Sample IGM#6 corresponds to an advanced "lit-par-lit" replacement of the chloritic shale by chalcopyrite. Samples IGM#7 and #8 are the most representative of the so-called *rubané* tin ores formed in chloritic shales with intercalations of centimeter-sized boudins of cassiterite, mostly showing a chloritic alteration in the contact with the shale. The sulfides occur mostly as veinlets of second-generation pyrite II and chalcopyrite cutting across cassiterite. Replacement of cassiterite by later sulfides can be observed. Samples IGM#2, IGM#3 and IGM#4 were collected as discrete meter-size lenses enveloped by cassiterite (Gaspar 1991, 1996). These lenses lie between the top of the cupriferous massive sulfides (MC) of Corvo and in direct contact with the footwall of the *rubané* ore (Gaspar 1996). The cassiterite crystals may show striking growth-zoning and strong brecciation.

ANALYTICAL METHODOLOGY

The hand samples were prepared as 2.5-cm-diameter araldite (loaded with graphite) polished sections for study by reflected microscopy and SIMS analyses of the sulfide minerals for gold. Some polished sections also were examined by scanning electron microscopy (SEM). The high-grade tin concentrate was sieved into plus and minus 250-mesh fractions for the polished sections, and splits were further ground to –200 mesh for bulk assays. In addition, part of one hand sample was crushed to –200 mesh for bulk assays. The assays were done for Au and Ag using conventional Pb-collection-scorification with atomic absorption spectrometry finish. Arsenic was measured by inductively coupled plasma – atomic emission spectrometry (ICP–AES) following aqua regia digestion of 200 mg samples in a closed system (microwave pressure-digestion). Concentrations of Fe, Cu, Sn and Zn, in 100 mg samples, were measured by ICP–AES following fusion with sodium peroxide and digestion of the melt in nitric and hydrochloric acids. The amount of sulfur was measured by infrared absorption following sample combustion with a Leco sulfur analyzer.

Quantitative image analysis was done using a MP–SEM–IPS system at CANMET. The system consists of a KONTRON–IBAS image analyzer integrated with a JEOL 733 electron microprobe with wavelength-dispersion and energy-dispersion X-ray spectrometers. The image analysis was performed using back-scattered electron (BSE) images acquired at 20 kV and 15 nA. The brightness and contrast of a BSE image are related to the average atomic number of the minerals in the samples. Discrimination among the minerals in the sample was done solely on the basis of the gray level of the BSE images. Two image-analysis programs were used with these samples. The first program determined the quantities of pyrite, chalcopyrite, sphalerite, arseno-

pyrite, stannite, cassiterite, and a group of the non-sulfide gangue minerals comprising mainly quartz, kyanite, feldspars, iron oxides and pyroxene. This image analysis was performed with 49 back-scattered electron (BSE) images of each polished section. The images were acquired at magnifications of 60× and 200× for the +250 and −250 mesh fractions of the Sn concentrate, respectively, and the −200 mesh fraction of sample #8. The second image analysis program searched for visible grains of gold in each of the two polished sections. This program was run with a meander of 115 by 115 fields acquired at a magnification of 400×, with approximately 1×10^6 particles covered by this meander. Each image is checked by the program to determine whether it contains a grain with a gray level as bright as gold or gold minerals. If the image does not have the desired gray level, the sample stage is moved automatically to the adjacent field, and the next image is acquired. When the specified range of gray levels is detected, the grain or grains having those gray levels are scanned by the program with the electron beam and a WDS dot map for gold is obtained for each grain to determine if the grain contains gold, and if so, the coordinates of the field, and the images are stored. At the end of the run, each of the recorded fields is manually checked to verify the presence of gold. This search is capable of finding grains of gold as small as ~1 μm.

The secondary-ion mass spectrometry (SIMS) depth-profile analyses were done on selected grains of pyrite and arsenopyrite using a Cameca IMS-4f secondary ion mass spectrometer with a double-focusing magnetic sector. A Cs$^+$ primary ion beam with impact energy of 14.5 kV was used, and negative secondary ions were detected. All samples had previously been coated with a thin film of carbon to prevent charging. The experimental parameters and methodology were as outlined in Cabri & McMahon (1995) and Genkin et al. (1998). The minimum detection level (MDL), as determined on implant standards, varied on different days as follows: arsenopyrite (11, 26, and 109 ppb Au) and pyrite (19, 49 and 134 ppb Au). Ion images were acquired from the multichannel plate or fluorescent screen assembly using a Photometrics Series 200 CCD camera. All instrumental parameters remained identical to those used for the quantitative analyses with the exception of the contrast aperture, which was reduced to 100 μm to improve the lateral resolution of the images.

ORE MINERALOGY

The eight hand samples studied have variable proportions of ore minerals, but all are rich in cassiterite and show layering of ore minerals, some of which are deformed. Pyrite occurs in two generations; the earliest (pyrite I) is the least abundant in some samples, occurring as rounded spongy, colloform, and layered grains of variable size with corroded borders (Fig. 4) replaced by euhedral cubic to subhedral crystals of pyrite II (Figs.

5, 6). Arsenopyrite is relatively rare in some of the samples studied, but is fairly abundant in two samples that are relatively chalcopyrite-poor (#3 and #8), as shown in Figures 4 and 5. Arsenopyrite also occurs as remnant
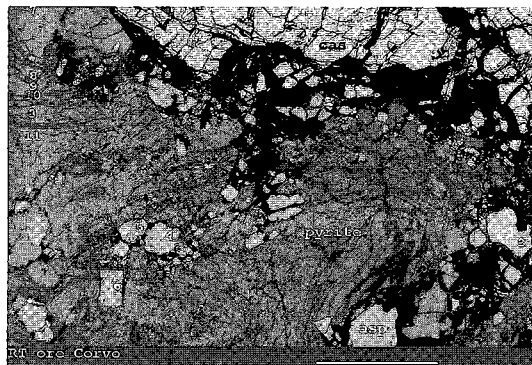

FIG. 4. Back-scattered electron (BSE) image showing banded and deformed pyrite II with isolated anhedral grains of arsenopyrite of variable size. The uppermost part of the image shows the edge of a millimeter-wide layer of cassiterite and some recrystallized pyrite II at the top left. The location of spots analyzed in arsenopyrite (Table 7) are indicated by numbers (2: NC–ASP2, 4: ASP4, 5: ASP5, 6: ASP6). The location of spots analyzed in pyrite (Table 6) are likewise indicated by numbers (7 and 8 represent pyrite II, NC–PY7 and 8; 3, 9, 10, and 11 represent pyrite I, NC–PY3, 9, 10 and 11). Scale bar: 1 mm.
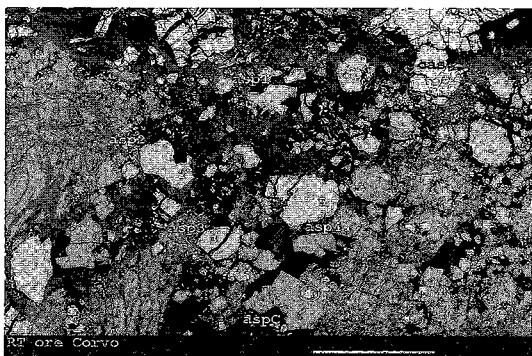

FIG. 5. BSE image partly overlapping Figure 4 showing variably-sized grains of arsenopyrite mostly concentrated in a poorly defined layer separating the cassiterite layer, shown at the top. Pyrite I is abundant, in places grading into pyrite II. The location of some spots analyzed in arsenopyrite (Table 7) is given by numbers (2: NC–ASP2, 3: NC–ASP3, and 5: NC–ASP5). The circle around a small inclusion of arsenopyrite in the lower part of the image encapsulates a grain of arsenopyrite included in pyrite II, for which ion images are given in Figure 7. Scale bar: 1 mm.

inclusions in pyrite II (Fig. 5). In these two samples, the arsenopyrite in some cases tends to occur in a zone between the cassiterite layer and the other sulfides (mainly pyrite), forming a distinct layer of relatively fine-grained crystals of arsenopyrite in one of the two samples. In some samples, chalcopyrite is the most abundant mineral within the layers mineralized with sulfides, occurring as large areas enclosing minerals such pyrite, tetrahedrite – tennantite, sphalerite, galena, arsenopyrite, and stannite. Chalcopyrite also fills fractures in crystals of second-generation pyrite (pyrite II), as shown in Figure 6, where it is closely associated with stannite. No native gold or electrum was observed in any of the samples studied. The eight samples were examined to select those most suitable for SIMS analysis on the basis of their sulfide mineralogy when compared to the mineralogy of the high-grade tin concentrate. Thus, the five samples selected (#1, 2, 3, 4, and 8) contain sparse chalcopyrite, abundant pyrite and cassiterite, with a variable content of arsenopyrite.

BULK ASSAYS AND IMAGE ANALYSES

The results of the bulk assays are given in Table 4, together with the calculated values for the tin-rich concentrate (based on the weights of the plus and minus 250-mesh fractions). The concentrations of Au, Cu, S and Zn are nearly identical, with Au slightly higher and S slightly lower in the combined tin concentrate. On the other hand, the concentration of Ag and As is substantially higher in hand-sample #8, and that of Fe is moderately higher, whereas that of Sn is obviously lower in the hand sample, even though it is a tin-rich sample. In

general, therefore, the bulk chemistry of the two samples is similar in terms of selected minor and trace elements. An unrelated Sn-rich (31% Sn) rubané sample from Neves–Corvo, analyzed by Activation Laboratories Ltd., gave an identical value to sample #8 for Au (130 ppb) and a similar value for As (5700 ppb), in addition to 1.6% Ta (M.D. Hannington, pers. commun., May, 1998). Quantitative image analysis was done to determine the modal weight percent of the minerals in the two sieved fractions of the Sn concentrate and sample #8 (Table 5).

RESULTS OF SIMS ANALYSES

A total of 55 pyrite grains from five hand samples and 23 arsenopyrite grains from three hand samples were analyzed for trace concentrations of gold, in addition to two grains of chalcopyrite and one of stannite, in which no gold was found. The pyrite grains were determined to be representative of either primary or secondary (recrystallized) generations prior to analysis on the basis of their morphology in polished section. In gen-

FIG. 6. BSE image showing a gradual change from pyrite I to large crystals of pyrite II and replacement of the latter by chalcopyrite and stannite. The location of spots analyzed in pyrite I (1, 2 and 4) (Table 2, PY1, 2, and 4) may be seen. A single spot-analysis was made of pyrite II (3: PY3, Table 6). Arsenopyrite occurs as rarer isolated grains in the top left, and fine-grained cassiterite is seen in the top right. Scale bar: 1 mm).

TABLE 4. RESULTS OF BULK ANALYSES OF THREE SAMPLES FROM NEVES-CORVO

Element		Sn conc. (+250 mesh) 30 g	Sn conc. (−250 mesh) 118 g	Sn Conc. Combined	Sample #8 42 g
Au	g/t	0.08	0.16	0.151	0.13
Ag	g/t	6.6	3.6	4.167	9.7
As	%	0.19	0.26	0.249	0.84
S	%	5.20	2.96	3.652	4.07
Fe	%	5.44	4.15	4.742	6.83
Cu	%	0.15	0.059	0.095	0.100
Sn	%	66.5	69.6	68.994	41.4
Zn	%	< 0.13	< 0.13	<0.13	< 0.13

TABLE 5. RESULTS OF IMAGE ANALYSES OF NEVES-CORVO TIN CONCENTRATE AND SAMPLE #8 (CORVO OREBODY)

Mineral	+250 mesh	−250 mesh	Sn concentration (combined)	Sample #8
cassiterite	89.9 %	88.7 %	88.9 %	56.5 %
pyrite	6.0	6.8	6.6	11.0
gangue*	3.6	3.5	3.5	29.5
arsenopyrite	0.3	0.8	0.7	2.1
stannite	-	-	-	0.1
chalcopyrite	0.2	0.1	0.1	0.2
sphalerite	0.1	0.1	0.1	0.1
Totals	100.1	100.0	99.9	99.5

* gangue: mainly quartz, feldspar, kyanite, Fe oxides and pyroxene.

eral, for all samples, arsenopyrite shows concentrations in the range from 0.036 to 2.719 g/t Au, and pyrite I, from 0.048 to 0.737 g/t Au, whereas pyrite II had either no gold detected or lower gold contents than in pyrite I for all individual samples. The results for pyrite and arsenopyrite are shown in Tables 6 and 7. In sample #1, concentrations of gold in pyrite I ranged from 0.135 to 0.240 g/t, and in pyrite II, from <0.019 to 0.040 g/t. For sample #2, concentrations of gold in pyrite I range from 0.082 to 0.289 g/t, and in pyrite II, gold was not detected (<0.019 g/t). In sample #3, concentrations of gold in pyrite II range from 0.061 to 0.152 g/t, with no grains of pyrite I found suitable for analysis. In sample #4, concentrations of gold in pyrite I range from 0.048 to 0.267 g/t, and in pyrite II, from <0.019 to 0.107 g/t. Average concentrations of gold for sample #8, on which we carried out most analyses, are as follows: 1.117 g/t (arsenopyrite), 0.504 g/t (pyrite I), 0.070 g/t (pyrite II). Average concentrations of gold for all grains analyzed for all samples are: 0.874 (arsenopyrite) and 0.183 g/t (pyrite I and pyrite II). In cases where no Au counts were recorded by SIMS, the average value for gold in pyrite was calculated by using one half the MDL, instead of using a zero value. Ion images were taken to determine the distribution of the gold in some grains of arsenopyrite as well as near their contact with other minerals. Figure 7 shows the distribution of gold along parallel layers in one grain of arsenopyrite for which a depth-

profile analysis gave 1.397 g/t Au (NC–ASP3, Table 7), as also shown in Figure 5, where the grain is seen in contact with pyrite. A small grain of arsenopyrite included in a crystal of pyrite II (Fig. 5) is separated by a sharp contact (Fig. 8A). Figure 8B shows that the gold is restricted to the arsenopyrite and is distributed heterogeneously in this case. Figure 9 shows evidence of heterogeneously distributed gold in arsenopyrite in contact with chalcopyrite. However, note that the arsenopyrite at the contact with chalcopyrite has no gold for a zone extending some 10 μm in width.

TABLE 7. RESULTS OF SIMS ANALYSES OF ARSENOPYRITE GRAINS FROM THE CORVO OREBODY

File No.	Sample	Au ppm	File No.	Sample	Au ppm
PY5=ASP	IGM#4	0.200	NC–ASP7	IGM#8	1.219
ASP–1	IGM#4	0.036	NC–ASP8	IGM#8	1.239
ASP–2	IGM#4	0.084	NC–ASP9	IGM#8	2.719
ASP–3	IGM#4	0.245	NC–ASP10	IGM#8	0.732
ASP–4	IGM#4	0.176	ASP1	IGM#8	1.543
ASP–5	IGM#4	0.386	ASP2	IGM#8	0.822
NC–ASP1	IGM#8	0.468	ASP3	IGM#8	1.613
NC–ASP2	IGM#8	1.052	ASP4	IGM#8	1.080
NC–ASP3	IGM#8	1.397	ASP5	IGM#8	1.660
NC–ASP4	IGM#8	1.228	ASP6	IGM#8	0.143
NC–ASP5	IGM#8	0.573	ASP7	IGM#8	1.278
NC–ASP6	IGM#8	0.216			

TABLE 6. RESULTS OF SIMS ANALYSES OF PYRITE GRAINS FROM THE CORVO OREBODY

| File	Sample	Generation	Au ppm	File	Sample	Generation	Au ppm
PY–23	IGM#1	II	0.021	PY–6	IGM#4	II	0.012
PY–24	IGM#1	I	0.135	PY–7	IGM#4	II	0.107
PY–25	IGM#1	I	0.194	PY–8	IGM#4	II	0.047
PY–26	IGM#1	II	NIL	PY–9	IGM#4	I	0.267
PY–27	IGM#1	II	0.040	PY–10	IGM#4	I	0.172
PY–28	IGM#1	I	0.240	PY–11	IGM#4	II	0.012
PY–29	IGM#1	I	0.166	PY–12	IGM#4	I	0.162
PY–30	IGM#1	II	NIL	PY–13	IGM#4	I	0.125
PY–31	IGM#1	I	0.205	PY–14	IGM#4	I	0.007
PY–32	IGM#1	II	NIL	PY–15	IGM#4	II	0.014
PY–33	IGM#2	II	0.013	NC–PY3	IGM#8	I	0.475
PY–34	IGM#2	I	0.193	NC–PY4	IGM#8	I	0.519
PY–35	IGM#2	I	0.261	NC–PY5	IGM#8	I	0.531
PY–36	IGM#2	II	0.013	NC–PY6	IGM#8	I	0.507
PY–37	IGM#2	I	0.082	NC–PY7	IGM#8	II	NIL
PY–38	IGM#2	I	0.289	NC–PY8	IGM#8	II	NIL
PY–39	IGM#2	I	0.142	NC–PY9	IGM#8	I	0.518
PY–16	IGM#3	II	0.120	NC–PY10	IGM#8	I	0.260
PY–17	IGM#3	II	0.061	NC–PY11	IGM#8	I	0.554
PY–18	IGM#3	II	0.078	PY1	IGM#8	I	0.372
PY–19	IGM#3	II	0.057	PY2	IGM#8	I	0.387
PY–20	IGM#3	II	0.152	PY3	IGM#8	II	0.082
PY–21	IGM#3	II	0.068	PY4	IGM#8	I	0.714
PY–22	IGM#3	II	0.100	PY7	IGM#8	I	0.737
PY–1	IGM#4	II	0.019	PY8	IGM#8	II	NIL
PY–2	IGM#4	I	0.054	PY9	IGM#8	I	0.476
PY–3	IGM#4	I	0.048	PY10	IGM#8	II	NIL
PY–4	IGM#4	II	0.025				
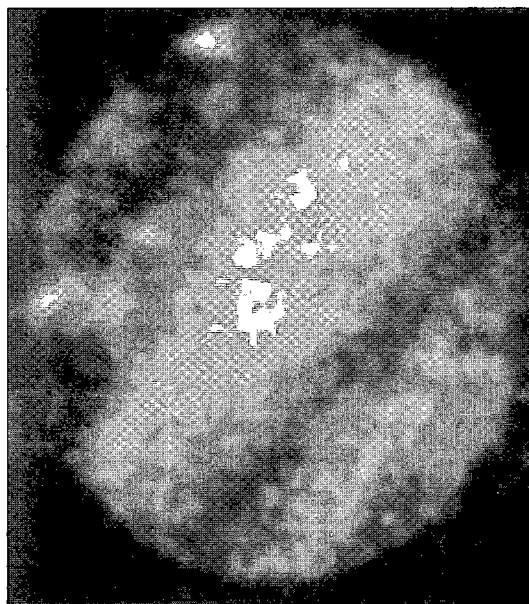
FIG. 7. Direct-ion image showing Au distribution as layers in a grain of arsenopyrite (NC–ASP3, Table 3, Fig. 5). This image and those in Figures 8 and 9 are 62.5 μm in diameter.
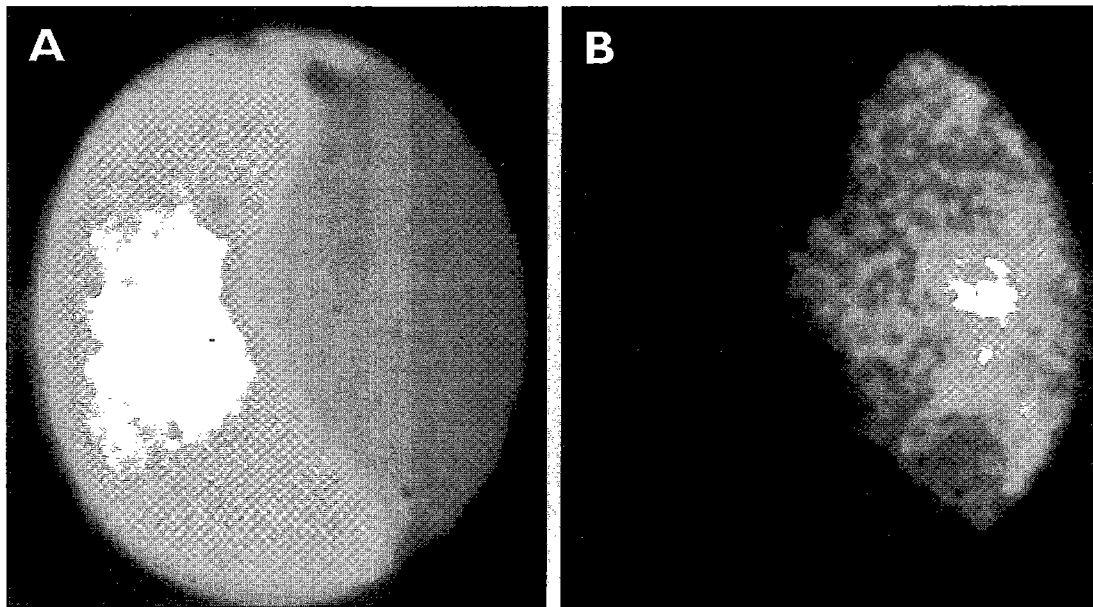
FIG. 8. (A) Direct-ion image of S at the contact between pyrite II (white) and arsenopyrite (gray), which is included (see Fig. 5). (B) Direct-ion image of Au for same area as in (A) showing Au in arsenopyrite only.

AUTOMATED SEARCH FOR VISIBLE GOLD
AND MINERALOGICAL BALANCE FOR GOLD

No gold grains were found by optical microscopy of all the polished sections. Also, the automated search for gold by image analysis of the plus and minus 250-mesh fractions of the Sn concentrate as well as of a polished section of a representative (–200 mesh) subsample of sample #8 did not locate any visible gold or gold-mineral grains. Instead, a few small inclusions of an unidentified Bi–Te–Se mineral (containing trace amounts of As and Pd) were found included in cassiterite.

A mineralogical balance for gold was calculated for the samples based on the SIMS analyses of pyrite I, pyrite II, and arsenopyrite, and the bulk assays, assuming these sulfides to be the only carriers of gold, using the modal proportions of the minerals determined by image analysis. In addition, it was estimated that the samples contain as much pyrite II as pyrite I, on the basis of optical observations. Thus, the calculated mineralogical balance for gold in the high-grade Sn concentrate (Fig. 10) shows that arsenopyrite and pyrite account for only 12% of the gold, and that the unaccounted portion is significant (88%). For sample #8, which is higher in As content and had the most sulfide grains analyzed by SIMS, invisible gold accounts for about 42% of the sample, distributed between arsenopyrite (18.0%), pyrite I (21.3%), and pyrite II (3.0%), leaving 57.7% unaccounted for, as shown in Figure 11.

Because there was no evidence of gold minerals in the samples studied, all the gold must reside invisibly in minerals, either as structurally bound gold or as subsurface submicroscopic grains of gold or gold minerals. We have determined in this study that gold occurs, in decreasing amounts, in arsenopyrite, pyrite I and pyrite II, and no gold was detected in two grains of chalcopyrite and one of stannite. The deposition of chalcopyrite, which is paragenetically later (Gaspar 1991), may also have been responsible for remobilization of a small amount of gold from arsenopyrite (Fig. 9). If no native gold or electrum is present in these samples, and if chalcopyrite and stannite are ruled out as potential carriers of gold, then one is left to speculate on the possibility of cassiterite being a carrier. Consideration of cassiterite as a possible host for gold is thus considered, though it is not known to be a carrier of gold (Cabri 1992), because it is the dominant mineral in the samples. Unpublished data (T. Seifert, pers. commun., 19 September, 1997) suggests that 14 ppm Au occurs in Neves – Corvo cassiterite, as determined by LAM–ICP–MS. Cassiterite has the rutile structure ($P4_2/mmm$). Möller et al. (1988) discussed coupled substitutions such as $W^{6+} + 2 Fe^{3+} = 3 Sn^{4+}$. Serranti (1998) reported average contents of 1,839 ppm W by micro-PIXE analyses (n = 11) and an average of 1.01 wt.% FeO by EPMA of cassiterite from the Corvo deposit. It is therefore possible to speculate on the substitution of Au^{3+} for Fe^{3+}, as is suggested for arsenopyrite (e.g., Johan et al. 1989).
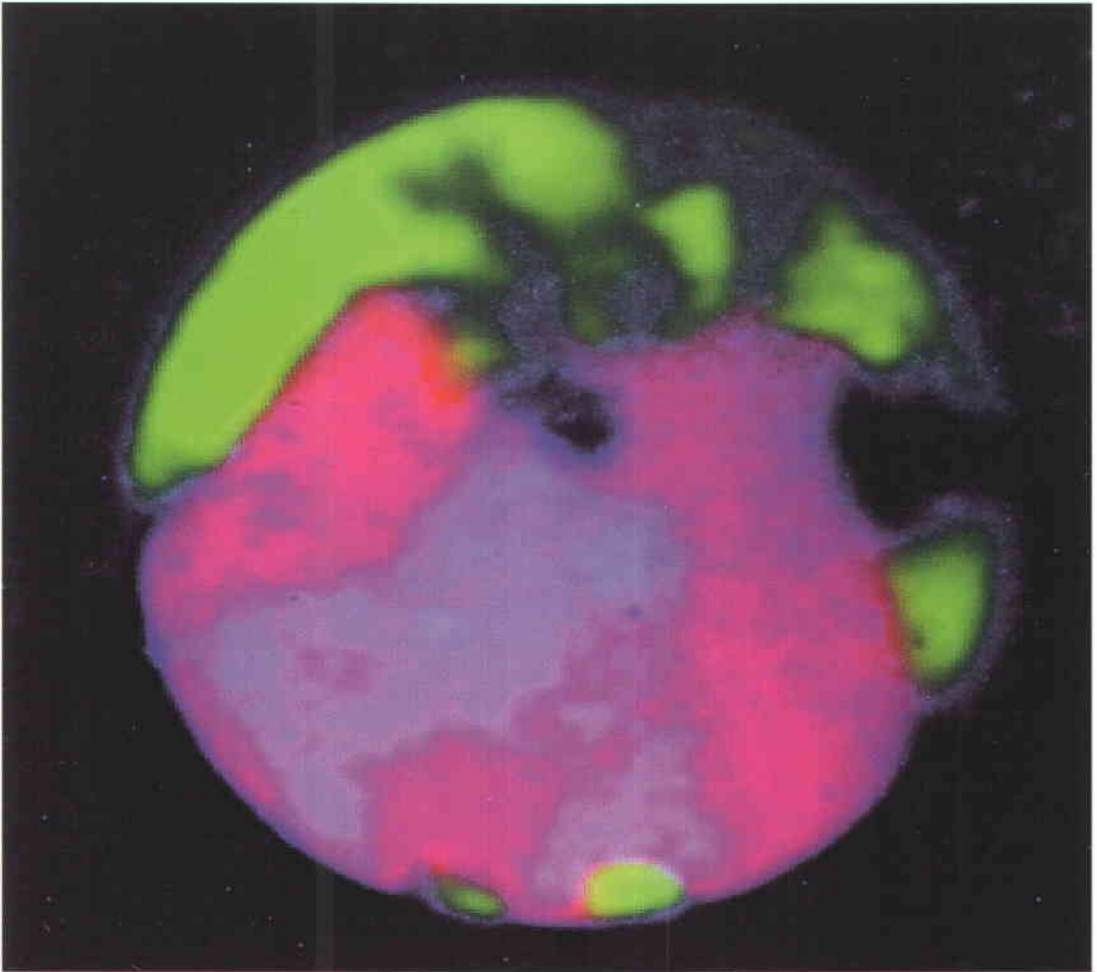
FIG. 9. Color overlay of direct-ion images showing the distribution of Au, Cu and As at the contact between arsenopyrite and chalcopyrite. Cu (green) at top of image is seen in contact with arsenopyrite (red), and the Au (blue) in arsenopyrite is missing for an approximate distance of 10 μm from the chalcopyrite contact.

Mineralogical balances, admittedly calculated with limited data, suggest that up to about 42% of the gold may be accounted for by arsenopyrite and pyrite for RT ore from the Corvo deposit. If one assumes that the missing gold occurs in the cassiterite structure, then the cassiterite in sample #8 contains about 133 ppb Au (57% of the total Au) and that in the high-grade Sn concentrate, a similar content, about 149 ppb Au (88% of the total Au).

DISCUSSION

Implications for mineral processing and metallurgy

Some observations may be made on the basis of this very limited study on the distribution of gold in the Corvo orebody. First, the high-grade Sn concentrate is a high-quality product in terms of Sn content, and it is also low in valuable elements such as Cu and penalty
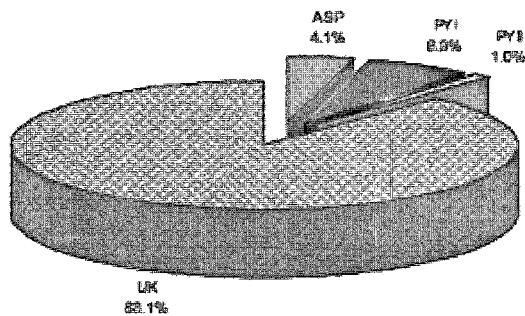
FIG. 10. Pie diagram showing the distribution of Au in minerals of the high-grade Sn tin concentrate; we make use of average results of all SIMS analyses of arsenopyrite (ASP) and pyrite, and assume that half the pyrite is pyrite I (PY I) and half is pyrite II (PY II). The unaccounted-for gold is shown by UK.
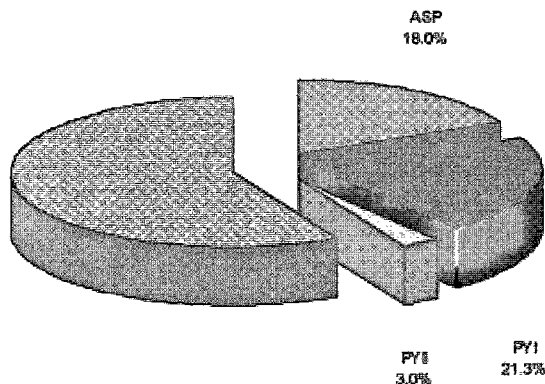

FIG. 11. Pie diagram showing the distribution of Au in minerals of sample #8; we make use of average results of SIMS analyses of arsenopyrite (ASP), pyrite I (PY I) and pyrite II (PY II), and assume that the missing gold is in cassiterite and that half the pyrite is pyrite I and half is pyrite II.

elements such as As. The gold content of the high-grade Sn concentrate is low (151 ppb), but similar to that of hand sample #8 (130 ppb), suggesting that the gold is concentrated in the Sn concentrate. However, the Au contents of cassiterite obtained by LAM–ICP–MS (T. Seifert, pers. commun., 1997) in preliminary studies seem very high with respect to our results but, in any case, were done on different samples. It may therefore be worthwhile to perform a more extensive investigation to determine the complete mineralogical balance because then options for recovery of the gold might be considered. The results of such a study may have implications for other polymetallic base-metal deposits where cassiterite is present, even though the quantities are minor (*e.g.*, Kidd Creek and Geco, Ontario).

For example, if the bulk of the gold resides invisibly in specific sulfides such as pyrite and arsenopyrite, it might be possible to break down the sulfides by roasting, followed by cyanidation to recover the gold. This procedure would have the advantage of reducing the amount of sulfur and arsenic in the feed to the furnace for cassiterite reduction. On the other hand, cyanide consumption may be high owing to residual sulfides, and rates of gold dissolution may be low. These potential problems may be controlled by a pre-cyanidation leach using lime and lead nitrate additions.

Another option might be to consider the smelting practice itself. When using reverberatory furnaces for smelting, the base of the furnace can slowly increase in thickness. Thus in the smelting for other metals, a significant part of the gold can slowly accumulate at the base of the furnace with time. The gold can then be recovered in different ways. One option could be to break up the furnace bottom when the furnace is scheduled for major maintenance, crushing it and processing it separately. Alternatively, intermittent runs could be

scheduled so that the operating conditions of the furnace are changed to melt part of the material accumulated at the base and tap it out.

Metallogenetic implications

These analytical results are the first to suggest the possibility that cassiterite may be a carrier of gold in the VMS of the Iberian Pyrite Belt. The genesis and the kind of occurrence of cassiterite have been a major problem at Neves–Corvo, which remains to be solved. Recently, Marcoux (1998) also concluded that the origin and the original depositional context of the cassiterite still need to be satisfactorily established. However, from isotopic data, Marcoux (1998) has excluded a pre-Paleozoic origin for the cassiterite, assuming that cassiterite deposition occurred only very soon after that of the massive sulfides at Neves–Corvo. The spatial distribution of the tin mineralization in the different orebodies seems to be confined by the major tectonic accidents that followed the same N–NE trend (Richards & Ferreira 1992). However, systematic mineralogical and textural studies of the different orebodies show different generations and mineralogical associations for both tin carriers: cassiterite (2/3 of the total Sn content of the deposit) and the tin sulfides (Gaspar 1991, 1996, Pinto *et al.* 1997).

Some controversy also exists concerning both the genesis and the actual structural position of the *rubané* ores. Therefore a comparison with results already published for the stringer and massive sulfide ores cannot be established. However, the cassiterite of the tin-rich rubané ore (RT) is quite different to that observed in the rich tin-bearing cupriferous massive ore (MS ore), in

terms of grain size, crystal growth and mineral associa-
tion. The smaller crystals of cassiterite (<150 μm) are
invariably associated with euhedral sphalerite in the MS
ores, whereas in the RT ore, sphalerite has not, so far,
been found close to the crystals of coarser cassiterite,
which are usually ≥200 μm in size (Gaspar 1991).

The colloform pyrite I, which always shows higher
gold contents than the recrystallized pyrite II (where not
affected by the later Hercynian deformation), always
occurs concordantly to the S_0 foliation of the black
shale. Also, because no halo indicative of a reaction
between pyrite I and the sediment has ever been ob-
served, it may be assumed that both were formed
syngenetically. On the contrary, however, infiltration of
hydrothermal tin-rich fluids usually produced a halo at
the contact with the slates, which is suggestive of sig-
nificant carbonate metasomatism of the rocks.

CONCLUSIONS

Study of a small number of samples from the Corvo
deposit, using a combination of quantitative methods of
analysis, has shown that arsenopyrite, pyrite I and py-
rite II are gold carriers. This study has also shown that
these minerals account for up to about 42% of the gold
in one sample of rubané tin-rich ore. The data also sug-
gest that cassiterite is the most likely carrier to account
for the missing balance of the gold in this sample. Ex-
trapolation of this approach to a high-grade tin concen-
trate, in order to arrive at a mineralogical balance for
gold, suggests a similar deportment of the gold. In the
case of the tin concentrate, however, the calculated
mineralogical distribution of gold is numerically differ-
ent. More precise data can be obtained with a more com-
prehensive study.

ACKNOWLEDGEMENTS

REFERENCES

CABRI, L.J. (1992): The distribution of trace precious metals in
minerals and mineral products. *Mineral. Mag.* **56**, 289-308.

_____ & McMAHON, G. (1995): SIMS analysis of sulfide
minerals for Pt and Au: methodology and relative sensitiv-
ity factors (RSF). *Can. Mineral.* **33**, 349-359.

CARVALHO, D., CONDE, L., HERNANDEZ ENRILE, J., OLIVEIRA,
V. & SCHERMERHORN, L.J.G.S. (1976): III Reunião de
Geologia do Sudoeste do Maciço Hespérico da Península
Ibérica, Huelva – Beja, 1975, Faixa Piritosa Ibérica. *Com.
Serv. Geol. Portugal* **LX**, 271-315.

FERREIRA, A., PINTO, A. & BOWLES, J.F.W. (1997): The occur-
rence of gold in the Neves – Corvo ore deposit, Portugal. In
SEG Field Conference 1997 (F.J.A.S. Barriga, ed.), Lis-
bon, Portugal (abstr.; 91).

GASPAR, O.C. (1991): Paragenesis of the Neves–Corvo
volcanogenic massive sulfides. *Comunicações, Serviços
Geológicos de Portugal* **77**, 27-52.

_____ (1996): Microscopia e petrologia de minérios
aplicadas à génese, exploração e mineralurgia dos
sulfuretos maciços dos jazigos de Aljustrel e Neves–Corvo.
Estudos, Notas e Trabalhos do IGM **38**, 195 p.

_____ (1998): Ore microscopy applied to the beneficiation
of volcanogenic massive sulfides. *Expl. Mining Geol.* (in
press).

_____ & PINTO, A. (1993): Neves – Corvo, a Kuroko type
deposit in the Iberian Pyrite Belt. *Proc. 29th Int. Geol.
Congress (Kyoto), J. Res. Geol., Spec. Issue* **17**, 249-262.

GENKIN, A.D., BORTNIKOV, N.S., CABRI, L.J., WAGNER, F.E.,
STANLEY, C.J., SAFONOV, Y.G., McMAHON, G., FRIEDL, J.,
KERZIN, A.L. & GAMYANIN, G.N. (1998): A multi-
disciplinary study of invisible gold in arsenopyrite from
four mesothermal gold deposits in Siberia, Russian Fed-
eration. *Econ. Geol.* **93**, 463-487.

HANNINGTON, M.D., BLEEKER, W. & KJARSGAARD, I. (1997):
Sulfide mineralogy, geochemistry, and ore genesis of the
Giant Kidd Creek Deposit. In *Geology and VMS Deposits
of the Iberian Pyrite Belt, SEG Neves Corvo Field Confer-
ence* (F.J.A.S. Barriga & D. Carvalho, eds.). *Soc. Econ.
Geol., Guidebook Ser.* **27**, 55-56.

HENNIGH, Q.T. (1996): *Geology of the Tin-Rich Orebodies of
the Corvo Deposit, Neves Corvo, Baixo Alentejo, Portugal.*
Ph.D. thesis, Colorado School of Mines, Golden, Colorado.

_____ & HUTCHINSON, R.H. (1997): Geology of tin-rich ore
of the Corvo orebody, Neves – Corvo deposit, Portugal. In
*Geology and VMS Deposits of the Iberian Pyrite Belt, SEG
Neves Corvo Field Conference* (F.J.A.S. Barriga & D.
Carvalho, eds.). *Soc. Econ. Geol., Guidebook Ser.* **27**, 96.

JOHAN, Z., MARCOUX, E. & BONNEMAISON, M. (1989):
Arsénopyrite aurifère: mode de substitution de Au dans la
structure de FeAsS. *C.R. Acad. Sci., Paris* **308**, *Sér.* **II**,
185-191.

LEISTEL, J.M., BONIJOLY, D., BRAUX, C., FREYSSINET, P.,
KOSAKEVITCH, A., LECA, X, LESCUYER, J.L., MARCOUX, E.,
MILÉSI, J.-P., PIANTONE, P., SOBOL, F., TEGYEY, M.,
THIÉBLEMONT, D. & VIALLEFOND, L. (1994): The massive
sulfide deposits of the South Iberian Pyrite Belt province:
geological setting and exploration criteria. *BRGM Doc.*
234, 236 pp.

_____, MARCOUX, E., DESCHAMPS, Y. & JOUBERT, M. (1998a): Antithetic behaviour of gold in the volcanogenic massive sulfide deposits of the Iberian Pyrite Belt. *Mineral. Deposita* **33**, 82-97.

_____, _____, THIÉBLEMONT, D., QUESADA, C., SÁNCHEZ, A., ALMODÓVAR, G.R., PASCUAL, E. & SÁEZ, R. (1998b): The volcanic-hosted massive sulfide deposits of the Iberian Pyrite Belt. Review and preface to the Thematic issue. *Mineral. Deposita* **33**, 2-30.

MARCOUX, E. (1998): Lead isotope systematics of the giant massive sulphide deposits in the Iberian pyrite belt. *Mineral. Deposita* **33**, 45-58.

_____ & LEISTEL, J.M. (1996): Mineralogy and geochemistry of massive sulfide deposits: Iberian Pyrite Belt. *Bol. Geol. y Minero*, **107**(3), 317-326.

MARKHAM, N.L. (1968): Some genetic aspects of the Mt. Lyell mineralization. *Mineral. Deposita* **3**, 199-221.

MÖLLER. P., DULSKI, P., SZACKI, W., MALOW, G. & RIEDEL, E. (1988): Substitution of tin in cassiterite by tantalum, niobium, tungsten, iron and manganese. *Geochim. Cosmochim. Acta* **52**, 1497-1503.

NEIVA, A.M.R. (1996): Geochemistry of cassiterite and its inclusions and exsolution products from tin and tungsten deposits in Portugal. *Can. Mineral.* **34**, 745-768.

OLIVEIRA, J.T., PACHECO, N., CARVALHO, P. & FERREIRA, A. (1997): The Neves Corvo mine and the Paleozoic geology of southwest Portugal. In *Geology and VMS Deposits of the Iberian Pyrite Belt, SEG Neves Corvo Field Conference* (F.J.A.S. Barriga & D. Carvalho, eds.). *Soc. Econ. Geol. Guidebook Ser.* **27**, 21-71.

PINTO, A., BOWLES J.F.W. & GASPAR, O.C. (1994): The mineral chemistry and textures of wittichenite, miharaite, carrollite, mawsonite, and In–Bi–Hg tennantite from Neves–Corvo (Portugal). *16th Int. Mineral. Asooc., Gen. Meeting (Pisa), Abstr.*, 329.

_____, FERREIRA, A. & BOWLES, J.F.W. (1995): Caracterização de minerais raros do jazigo de Neves–Corvo e suas implicações metalogénicas. *IV Cong. Nac. Geol. (Porto), Abstr.*, 665.

_____, _____, _____ & GASPAR, O.C. (1997): Mineralogical and textural characterisation of the Neves–Corvo ores: metallogenic implications. In *Geology and VMS Deposits of the Iberian Pyrite Belt, SEG Neves Corvo Field Conference* (F.J.A.S. Barriga & D. Carvalho, eds.). *Soc. Econ. Geol., Guidebook Ser.* **27**, 90 (abstr.).

_____, _____, _____ & _____ (1997): Mineralogical and textural characterization of the Neves – Corvo ores. Metallogenic implications. In *SEG Field Conference 1997* (F.J.A.S. Barriga, ed.). Lisbon, 90.

REAL, R. & CARVALHO, P. (1997): GEOMMINCOR: successful scientific – industrial interaction in the geological investigation of the Neves Corvo mineral deposits. In *SEG Field Conference 1997* (F.J.A.S. Barriga, ed.). Lisbon, 84.

RELVAS, J.M.R.S., PINTO, A., BARRIGA, F.J.A.S., FERREIRA, A. & NOIVA, P.C. (1997): Geological, textural and paragenetic relationships among copper, tin and copper – tin ores from the Corvo orebody, Portugal. In *Geology and VMS Deposits of the Iberian Pyrite Belt, SEG Neves Corvo Field Conference* (F.J.A.S. Barriga & D. Carvalho, eds.). *Soc. Econ. Geol., Guidebook Ser.* **27**, 94-95 (abstr.).

RICHARDS, D.G. & FERREIRA, A. (1992): Metal zoning in Graça, Neves – Corvo. *Minerals Ind. Int.,* 5-9.

SERRANTI, S. (1998): *Le mineralizzazioni "rubané" e massiva del giacimento a Cu–Zn di Corvo (Neves–Corvo, Portogallo): studio metallografico e geochimico, implicazioni genetiche e applicazione di tecniche di analisis d'imagine.* Ph.D. thesis, Università degli Studi di Roma "La Sapienza", Roma. Italia.

_____, FERRINI, V. & MASI, U. (1997): Micro-PIXE analyses of trace elements in ore minerals from the Neves–Corvo deposit (Portugal): preliminary report. In *SEG Field Conference 1997* (F.J.A.S. Barriga, ed.). Lisbon, 96.